ELSEVIER

Earth and Planetary Science Letters 136 (1995) 109–121

EPSL

Experimental and theoretical studies of the stabilities of talc, antigorite and phase A at high pressures with applications to subduction processes

Kunal Bose [a], Jibamira Ganguly [b,*]

[a] *Department of Geological and Geophysical Sciences, Princeton University, Princeton NJ 08544, USA*
[b] *Department of Geosciences, University of Arizona, Tucson AZ 85721, USA*

Received 17 May 1995; revised 11 August 1995; accepted 28 September 1995

Abstract

We have experimentally determined the equilibrium talc ⇄ enstatite + quartz/coesite + H_2O to 40 kbar in the system $MgO–SiO_2–H_2O$ (MSH) using both synthetic and nearly pure Mg end-member natural talc and other synthetic starting materials for the other solid phases. At 40 kbar, the equilibrium dehydration boundary lies ~ 150°C higher than that calculated using data from the existing internally consistent thermochemical data bases. The reason for this discrepancy lies in the erroneous compressibility data of talc in the data bases. We have retrieved the compressibility of talc from the experimental phase equilibrium data, and have also calculated several other equilibria in the MSH system involving talc, antigorite and the dense hydrous magnesium silicate (DHMS), commonly referred to as phase A. Comparison of these equilibria with selected thermal profiles at the leading edge of young and old subducting oceanic slabs, along with the dehydration condition of basaltic amphibole and solidus of mantle peridotite, provides an explanation for the observed heights of the volcanic fronts above subducting oceanic lithosphere. Further, it is found that in cold oceanic slabs (≥ 50 Ma with subduction velocity of ≥ 10 cm/y), antigorite will transform to the DHMS phase A through a vapor conserved reaction at a depth of ~ 200 km. Phase A will then serve as a carrier of water into the deeper mantle.

1. Introduction

The system $MgO–SiO_2–H_2O$ (MSH) has received considerable attention from petrologists and mineralogists since it was first studied by Bowen and Tuttle [1]. Among the phyllosilicates whose dominant end-member compositions belong to the MSH system, talc is a major phase of considerable geological importance. It occurs in eclogite facies metamorphic rocks, high-grade pelitic blueschists [2], whiteschists [3] and in high-pressure crystalline basement and ophiolitic cover rocks (e.g. the Dora Maira Massif of the Western Alps, [4,5]). It is ubiquitous in metamorphosed ultramafic rocks, in subduction zone environments [6–8], submarine hydrothermal systems and surface environments [9]). However, there has been very little experimental study on the stability relations of talc at $P > 13$ kbar, even though many of the interesting applications of the equilibrium relations of talc to geological problems fall in much higher pressure regimes (e.g. [10,11]). The present work was primarily undertaken to fill this

* Corresponding author.

SSDI 0012-821X(95)00188-3

gap in the experimental database by determining the equilibrium talc = 3 enstatite + quartz/coesite + H_2O to ~ 45 kbar, and to retrieve a set of thermodynamic properties of talc that are consistent with the new experimental data. In addition, we have also calculated the equilibrium talc + kyanite = pyrope + 2 coesite + H_2O and the approximate stability relations of antigorite and of the dense hydrous magnesium silicate (DHMS) $Mg_7Si_2O_8(OH)_6$, which is commonly referred as phase A. The integrated phase diagram in the MSH system has then been applied to oceanic subduction processes, specifically to explain the height of volcanic fronts above the Benioff zone and to understand the conditions under which water may be recycled into the deep mantle.

2. Experimental studies

2.1. Experimental procedure: P–T measurement

All experiments were conducted in an end-loaded piston cylinder apparatus using 1/2′ (1.27 mm) internal diameter WC (13% Co binder) cores, WC (6% Co binder) pistons, and salt pressure cells similar to those used by Bose and Ganguly [21]. The experimental procedure followed in this work was also essentially similar to that in [21]. Detailed analysis of the friction characteristics [21] in our experimental set up and procedure shows that the friction decays almost completely after ~ 40 h at the temperature of our experiments. During this process, there is a progressive drop of nominal pressure towards a steady-state value, which represents the true sample pressure. Thus, except for one, the duration of all experiments exceeded 40 h and the final nominal pressure was accepted as the true sample pressure.

Pressure was monitored by a 16 inch (406.4 mm) diameter Heise gauge, calibrated to NBS standards, and also by an on-line digital pressure transducer. The thermocouple (W-3Re/W-25Re) signal was pre-amplified by a 100X instrumentation amplifier (maximum gain error 0.02%) and the thermocouple cold-junction was corrected with a cold-junction correction integrated circuit (maximum error 0.5°C). The e.m.f. of the thermocouple was also measured before the preamplifier and cold junction correction by a calibrated digital voltmeter with a resolution of 0.01 mV. In the absence of any directly measured data, no correction was made for the pressure effect on W/Re thermocouples. However, corrections made according to Lane and Ganguly [12] suggest that the true temperature should be a little higher than the nominal temperature, but by no more than 5°C. The experiments were quenched by shutting off the power to the graphite furnace in the pressure cell.

2.2. Starting materials and reversal procedure

We have constrained the equilibrium dehydration boundary of talc by 'reversal' of the direction of reaction. The starting mixture consisted of synthetic orthopyroxene plus quartz or coesite (depending on the pressure), along with either natural or synthetic talc. The natural talc was collected from Gouverneur, New York. Electron microprobe analysis showed it to be essentially a Mg end-member, with the chemical formula $(Mg_{\cdot 99}Fe_{\cdot 01})_3Si_4O_{10}(OH)_2$. Talc was also synthesized hydrothermally at 2 kbar, 640°C (2–4 days) from stoichiometric mixtures of MgO (99.99%) and synthetic cristobalite, which were sealed with excess water in 0.5′ (12.7 mm) diameter Au capsules. Grain sizes of the synthetic talc were between 1 and 2 μm. Ortho-enstatite was synthesized in two stages. Stoichiometric amounts of MgO and cristobalite were mixed, pelletized, and heated at 1450°C for 4 h in a graphite container in an 1 atm furnace. Ar gas was purged through the furnace to prevent the graphite container from burning. The quenched product was ground in an agate mortar, repelletized, and heated for an additional 20 h. X-ray diffraction showed the product to be a mixture of clino- and proto-enstatite. This product was then held at 1150°C, 20 kbar for 4 days, which resulted in its complete conversion (within the resolution of X-ray diffractometer scans) to 15–20 μm size prismatic crystals of pure ortho-enstatite.

Notes to Table 1:
Ta = talc; OPx = orthopyroxene; Coes = coesite; 10Å = 10Å phase. * Starting material: talc, enstatite, quartz/coesite (*all Synthetic*) + H_2O. † Starting material: *natural* talc, *synthetic* enstatite, quartz/coesite + H_2O. + + = Strong (> 90%) growth; - - = strong decay.

Table 1
Experimental conditions and results for talc dehydration equilibrium

Run#	T, °C	P, kbar	Duration, hrs	Result
TLC1	700	38.5	36	* Ta++, OPx--, Coes-- † Ta++, OPx--, Coes--
TLC3	740	38	54	* Ta++, OPx--, Coes-- † 10Å, minor Opx, Coes
TLC4	770	38	71.5	* Ta++, OPx--, Coes-- † Ta
TLC11	800	37.9	72	* Ta++, OPx--, Coes-- † Ta
TLC6	830	38	45	* OPx++, Coes++ † OPx++, Coes++
TLC9	820	36.5	51	* OPx++, Coes++ † 10Å, Opx, Coes
TLC8	800	36.1	45	* Ta++, Coes-- † Ta++, OPx--, Coes--
TLC12	815	35.9	72	* OPx++, Coes++, Ta-- † Ta++, Coes--
TLC26	775	43.05	69.25	*Ta+, OPx-, Coes-
TLC27	795	47.02	70	*Ta--, OPx++, Coes++
TLQ13	805	29	71.5	* Ta † Ta++, minor Qz
TLQ14	820	28.3	69	* Ta † Ta++, minor Qz, OPx
TLQ15	840	28.7	46	* OPx, Qz++, Ta-- † Ta++, Qz--, OPx--
TLQ22	825	24.5	72	* Ta
TLQ23	835	24	118	* OPx++, Qz++, Ta-- † Ta
TLQ24	840	24	70	† OPx++, Qz++
TLQ18	850	21.3	82	* OPx, Qz † Ta++, no Qz, minor OPx
TLQ16	820	20	59	* Ta † Ta
TLQ19	830	20	55	* OPx, Qz
TLQ17	840	19.7	71	* OPx, Qz † OPx, Qz
TLQ20	815	16.3	74.5	*Ta † Ta
TLQ21	830	16.2	77.5	* OPx, Qz † Ta++, minor OPx, Qz
TLQ25	850	16.3	70	† OPx, Qz

For determination of the reaction Talc = 3 enstatite + SiO_2 + H_2O, a mixture of approximately stoichiometric amounts of either synthetic or natural talc and enstatite, along with ~ 10% excess quartz or coesite (depending on which polymorph is stable at the desired experimental condition), was sealed with excess distilled H_2O in gold capsules. Excess quartz was used to compensate for its dissolution in H_2O at the experimental P–T conditions. The presence of free quartz in the experiments should also have ensured that both synthetic and natural talc were silica saturated. Each experiment consisted of two sealed capsules, one containing ~ 1.0 μm size fraction of natural talc and the other containing synthetic talc (1–2 μm). Both capsules were placed next to each other at the central segment of the graphite resistance furnace, which constitutes its 'hot-spot'. Earlier work in our laboratory showed no significant temperature gradient across the height of the sample capsules within the pressure cells. Reaction directions were followed by noting the change of the relative X-ray peak intensities of the product and reactant phases in the experimental product from those in the starting material. Only those experiments in which the capsules recovered after quenching showed the presence of water were considered successful. All reactions reported here showed at least 25% change in the peak height ratios in the XRD pattern between the starting mixture and the experimental product.

2.3. Experimental results and discussion

The experimental results for the reaction Talc = 3 enstatite + SiO_2 + H_2O, using both synthetic and natural talc as starting materials, are summarized in Table 1, and illustrated in Fig. 1a. The equilibrium dehydration boundary of synthetic talc has been found to be systematically lower than that of natural talc by ~ 10–15°C. The compositions of talc and enstatite in the quenched run products, as determined by electron microprobe, show that the observed difference between the stability of synthetic and natural talc cannot be due to the effect of solid solution. Thus, the synthetic talc must have had slightly higher free energy, which was most likely due to a somewhat higher defect density compared to that in the natural talc, especially since both types of talc had similar grain size (1–2 μm), which rules out differential contributions from surface free energy. The measured value of the surface free energy of talc [13] [Giese, pers. commun.] shows that the surface free energy contribution has a vanishingly small effect on the stability of either natural or synthetic talc at the grain size employed in our work.

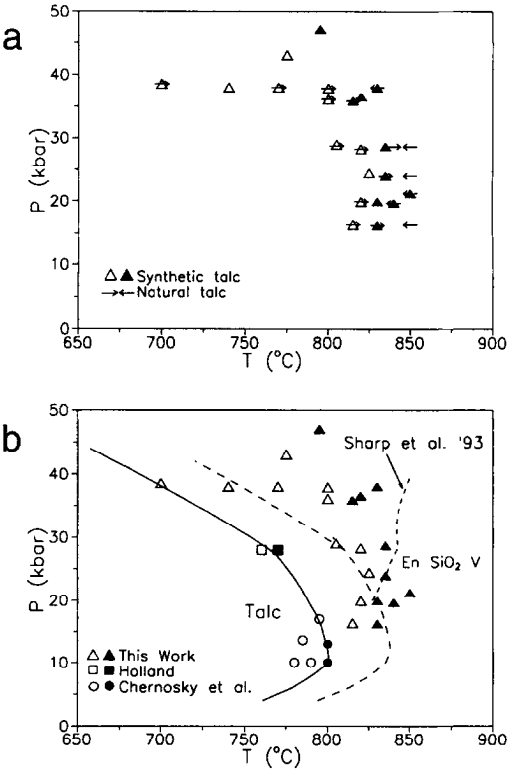

Fig. 1. (a) Experimental data on the equilibrium Talc = 3 Enstatite + SiO_2 + H_2O. Triangles indicate experiments with synthetic talc; △ = talc growth, ▲ = talc breakdown. The arrows indicate experiments with natural talc with the direction of arrows pointing towards the direction of reaction. (b) Summary of selected experimental data on the stability limit of synthetic talc and comparison with calculations of the stability limit from thermochemical data. Triangles = this work; circles = Chernosky et al. [14]; squares = Holland, quoted in [14]. Open symbols = growth of talc; filled symbols = growth of enstatite + quartz/coesite. Solid line = calculation of the stability of talc according to the thermochemical data base of Berman [16]. A very similar result is obtained from the data base of Holland and Powell [15]. The large dashed line illustrates the effect of changing the heat of formation (from elements) of talc to −5900 kJ/mol, as suggested by Hemingway [27]. The small dashed line represents the calculation by Sharp et al. [24] by assuming a linear compressibility of talc of 2.42 Mb^{-1}. The kink on the latter curve near 30 kbar is due to quartz/coesite transition. All other kinks are artifacts of the graphics program.

The experimental results for the stability limit of synthetic talc, as determined in this work, have been compared in Fig. 1b with those of Chernosky et al. [14] and Holland, which was quoted in [14] as a personal communication. Also shown is the calculated P–T location of the equilibrium Talc = 3 enstatite + SiO_2 + H_2O according to the widely used thermodynamic data of Holland and Powell [15] and Berman [16]. It is evident that, according to our experimental data, talc has a much higher thermal stability than that calculated from these thermodynamic data. The unpublished experimental reversal of Holland at 28 kbar, which seemed to have been used as a constraint in the derivation of thermodynamic properties of talc in these data bases, is ~ 70°C lower than the equilibrium dehydration boundary of talc determined in this study at the same pressure. Our data are consistent with those of Kitahara et al. [17] at 20 kbar and Thompson and Ellis [18] at 25 kbar, and show that the thermal maximum on the equilibrium dehydration boundary of talc is ~ 25 kbar instead of the ~ 10 kbar that is predicted from the thermochemical data. We present below an analysis of the thermodynamic properties of the phases involved in the dehydration equilibrium of talc, and retrieve a set of values which are consistent with our 'reversal brackets'. Throughout this work, the standard state for the solid phases has been chosen to be the pure state at 1 bar, T.

For H_2O, the choice of available high pressure equation of state, such as those of Delany and Helgeson [8], Belonoshko and Saxena [19] and Brodholt and Wood [20], does not affect the position of the equilibrium up to 40 kbar by more than 5°C. The calculated P–T condition for brucite dehydration equilibrium using any of the three equations of state is in excellent agreement with the experimental data to 40 kbar. The thermochemical properties of enstatite, quartz and coesite are well constrained [15,16,21]. We, thus, conclude that the discrepancy between the experimentally determined and calculated P–T conditions of the talc dehydration equilibrium must lie in the thermodynamic properties of talc itself. The thermochemical properties of talc retrieved by various workers from the phase equilibrium data [15,16,22,23] are summarized in Table 2, and compared with the calorimetric data [26,27]. There is excellent agreement between the retrieved and calorimetric values of entropy of talc, except for the results of Day and Halbach [22], which used a very restricted set of reversal brackets, but that there is significant variation in the enthalpy of formation (ΔH_f°) values of talc. However, as illustrated in Fig. 1b, the effect of reducing the ΔH_f° value for talc is simply to shift the dehydration boundary to higher temperature without significant change of its form, including the pressure of the thermal maximum. We, therefore, conclude that the reason behind the discrepancy between the calculated and experimentally determined dehydration boundary of talc lies in its

Table 2
Enthalpy of formation from the elements (kJ/mol) and third law entropy of talc at 1 bar, 298 K in existing thermochemical databases [15,16,22,23], and as determined by calorimetric measurements [26,27], along with the values preferred in this work to be consistent with the phase equilibrium data

Source	ΔH_f (kJ/mol)	S (J/mol/K)
Berman [16]	-5897.387	261.24
Holland & Powell [15]	-5895.23 ± 3.7	260.80
Day et al. [23]	-5898.217	260.83
Day & Halbach [22]	-5906.569	269.53
Hemingway [27]	-5900 ± 2.0	260.83 ±0.
Bose [26]	-5897 ± 1.7	

volumetric property as a function of P and T (also see [24,25]), which has not been constrained by any experimental data on the thermal expansion and compressibility in the existing data bases.

3. Retrieval of thermodynamic properties of talc

3.1. Procedure

At equilibrium, the following equation must be satisfied for the dehydration of talc in the MSH system.

$$\Delta G(P,T) = \Delta H_s^\circ(1,T) - T\Delta_s^\circ(1,T) + \int_1^P (\Delta V_T^\circ)_s \mathrm{d}P + G_{H_2O}^\circ(P,T) = 0 \quad (1)$$

where the subscript s stands for solid phases, the superscript o denotes pure phase, and $(\Delta V_T^\circ)_s$ stands for the stoichiometric volume change of the solid phases in the reaction at the temperature of interest, T. Using this relation, a self-consistent set of thermodynamic parameters for talc, which are compatible with our experimental 'reversal brackets', was retrieved as follows:

(1) The thermodynamic properties (H°, S°, Cp°, $V^\circ(T,P)$) of enstatite and β-quartz (which is the stable polymorph formed by the dehydration of talc) were taken from Berman [16], whereas the H° and S° values for coesite were from the recent work of Bose and Ganguly [21], who retrieved these properties from a careful determination of the quartz-coesite equilibrium between 500° and 1200°C, and using the thermochemical properties of quartz from Berman [16]. The G_{H_2O} data were taken from Delany and Helgeson [8] in order to be consistent with the data base of Berman [16], although the use of the water property from either Belonoshko and Saxena [19] or Brodholt and Wood [20] would have had no significant effect on our calculations, as noted above.

(2) We have assumed that, for talc, the thermal expansion coefficient (α) and compressibility (β) can be expressed as linear functions of T and P, respectively ($\alpha = \alpha_0 + \alpha_1 T; \beta = \beta_0 + \beta_1 T$), and that $\alpha(T) \neq f(P)$ (which also implies that $\beta(P) \neq f(T)$) so that:

$$V(P,T) = V(1,298)\left[1 + \alpha_0(T-298) + 0.5\alpha_1(T^2 - 298^2) - \beta_0(P-1) - 0.5\beta_1(P^2-1)\right] \quad (2)$$

where α_0, α_1, β_0 and β_1 are constants. Integrating (2) and rearranging terms, we obtain:

$$\psi \equiv \frac{\int_1^P V_T(P)\mathrm{d}P}{V_{298}^0(P-1)} - 1 = C_0\alpha_0 + C_1\alpha_1 - C_2\beta_0 - C_3\beta_1 \quad (3)$$

where: $C_0 = T - 298$, $C_1 = (T^2 - 298^2)/2$ and $C_2 = (P-1)/2$, $C_3 = (P+2)(P-1)/6$.

(3) For talc, values of ΔH_{298}° and ΔS_{298}° are taken to be equal to their calorimetric values [26,27] (see Table 1). We have chosen not to use the values retrieved from phase equilibrium data for the sake of

Table 3
Volumetric parameters of talc and antigorite (Atg) that are compatible with the phase equilibrium data

	$\alpha_0(K^{-1})$	$\alpha_1(K^{-2})$	$\beta_0(bar^{-1})$	$\beta_1(bar^{-2})$	$\Delta H°(298)$	$S°(298)$
Talc	$2.606(10^{-5})$	0.0	$2.552(10^{-6})$	$-4.514(10^{-11})$	-5897.387	261.24
talc	$5.503(10^{-5})$	0.0	$4.664(10^{-6})$	$-1.336(10^{-10})$	-5900.000	260.83
Atg	$2.261(10^{-5})$	$7.885(10^{-9})$	$2.831(10^{-9})$	$-4.37(10^{-11})$	-71364.15	3603

The last two columns are the enthalpy (kJ/mol) and entropy (J/mol-K) values which go along with the thermal expansion and compressibility parameters. For talc, row 1: Bose et al. [26] for ΔH_f°(298 K) and Hemingway [27] for S°(298 K); row 2: Hemingway, [27] for both. Our preferred values are those in row 1 (see text). ΔH_f°(298 K) and S°(298 K) for antigorite are from Berman [16].

internal consistency, since we have not used the earlier phase equilibrium data in the retrieval of V as a function of P and T (see below for further discussion). Along with the other thermochemical properties discussed above, these values have been used to solve for the $\int V\mathrm{d}P$ term for talc, which was then converted to ψ, as defined in Eq. (3). Instead of choosing an arbitrary point within a 'reversal bracket' as an equilibrium P,T condition, the extrema of a reversal bracket were chosen to represent equally probable equilibrium conditions taking into account the uncertainties of P,T determinations (± 5°C and ± 0.2 kbar, respectively).

(4) The calculated values of ψ were subjected to multiple linear regression, using an SPSS proprietary software package [28], against the parameters C_0, C_1, C_2 and C_3, to retrieve α_0, α_1, β_0 and β_1. In order to be compatible with the form of Eq. (3), the regression was constrained to pass through the origin.

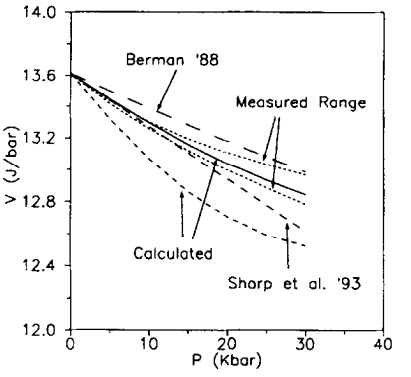

Fig. 2. Comparison of the retrieved (Berman [16], Sharp et al. [24], and this work) and measured [29,30] compressibility data of talc. Heavy solid line and dashed line (labelled as 'calculated') = this work — retrieved from the phase equilibrium data illustrated in Fig. 1a and thermochemical data (see text). Short dashed lines = measured range by Vaidya et al. [30] (upper line) and Vadiya and Kennedy [29] (lower line).

3.2. Results and discussion

The retrieved thermal expansion and compressibility values of synthetic talc are summarized in Table 3. Vaidya and Kennedy [29] and Vaidya et al. [30] determined the compressibility of natural talc to 30 kbar in a piston cylinder apparatus. The V–P relation dictated by the compressibility behavior of talc, as retrieved above, is compared with the experimentally determined V–P relations in Fig. 2. Also shown for comparison are the V–P relations retrieved by Berman [16]. We find that the compressibility of talc, which has been constrained by its $\Delta H_f^\circ(298)$ value from Bose et al. [26] and $S^\circ(298)$ value from Hemingway [27], lies within the range of its experimentally determined values. Consequently, we accept these thermochemical values (which are essentially the same as in the data base of Berman [16]), and the associated values of α and β (first row, Table 3) constrained by our experimental reversal brackets as the most reasonable self-consistent thermodynamic data set of talc. (Since this paper was submitted, we became aware of a new set of compressibility measurement of talc by Pawley et al. [31] and Pawley [pers. commun.] to 50 kbar, which are in excellent agreement with our preferred V–P relation, as illustrated by a solid line in Fig. 2.)

In an attempt to reconcile the differences between the thermodynamically predicted phase equilibria and existing experimental data involving talc (Ta = En + SiO_2 + H_2O; Ta + Ky = Py + Coes + H_2O; Chl + Ky + Ta = Py + H_2O) at $P > 20$ kbar, Sharp et al. [24] proposed that the compressibility of talc be changed to 2.42 Mb^{-1}. Although they were qualitatively correct in identifying the problem with the compressibility of talc in the data bases, their calculated equilibrium (using the database of Holland and Powell, [15]) for the reaction Talc = OPx + Qz/Coes + V does not match our experimental determination (Fig. 1b). Also, the resulting compressibility is well outside the experimental range [29,30], as illustrated in Fig. 2.

The calculated equilibrium boundary for the dehydration reaction Talc = 3 enstatite + SiO_2 + H_2O, using the preferred set of thermodynamic data of talc along with the properties of enstatite and quartz from Berman [16], of H_2O from Delany and Helgeson [8] and coesite from Bose and Ganguly [21], are compared with the experimental reversal brackets determined in this work and by Chernosky et al. [14] in Fig. 3. Our calculated equilibrium is in good agreement with the low pressure (0.5–2.0 kbar) hydrothermal reversal data of Chernosky et al. [14], but misses their data at 10–13 kbar, which were determined in a

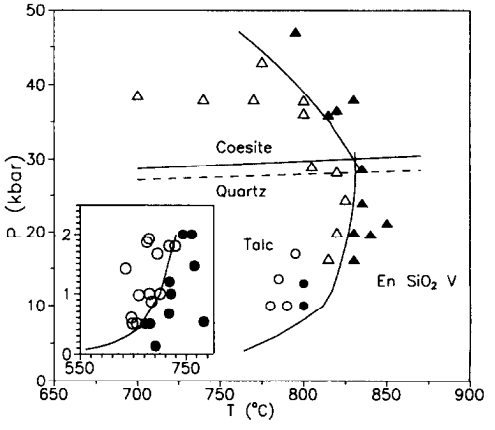

Fig. 3. Comparison of the calculated dehydration boundary of talc (talc = 3 enstatite + quartz + H_2O) according to the retrieved thermochemical data with the experimental data of this work (triangles) and Chernosky et al. [14] (circles). The data at $P \leq 2$ kbar are shown as an inset using an expanded scale for pressure. Open symbols = growth of talc; filled symbols = growth of enstatite + quartz. The solid line represents the result of calculation using the $\Delta H_f°$ and S° of talc from Bose et al. [26] and Hemingway [27], respectively, along with the retrieved α and β functions (Table 3). Kinks on the calculated equilibrium boundaries do not represent invariant points, but calculated points which are not smoothed out by the graphics program. The quartz–coesite equilibrium is according to Bose and Ganguly [21] (solid line) and Bohlen and Boettcher [46] (dashed line).

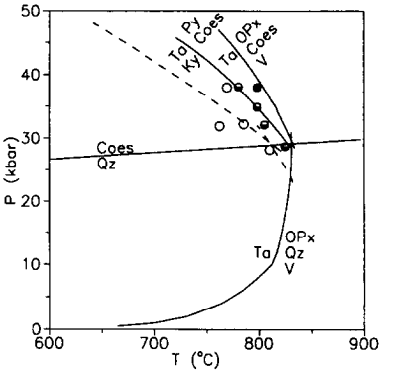

Fig. 4. Calculated locations of the equilibrium talc + kyanite = pyrope + 3 coesite + H2O (TKPCV) according to the thermodynamic properties of (a) talc derived in this work; (b) coesite from Bose and Ganguly [21]; and (c) the other phases from Berman [16] (dashed line) and Saxena et al. [32] (solid line). Also shown are the quartz–coesite transition from Bose and Ganguly [21] and the upper thermal stability of talc, as determined in this work. The circles represent the experimental data of Chopin [33] on the TKPCV equilibrium; open symbol = talc growth; filled symbol = talc breakdown; half-filled symbol = no reaction. The kink on the talc dehydration equilibrium at ~ 30 kbar is due to the quartz/coesite transition. All other kinks are represent calculated points which are not smoothed out by the graphics program.

piston cylinder apparatus, by ~ 10–15°C. The reason for this discrepancy is not clear, but may partly be related to the calibration of the pressure gauge and much smaller resolution of thermocouple e.m.f. reading in the latter study. We do not recommend optimization of our data with those Chernosky et al. [14] with equal weight since the two sets of data were collected with significantly different levels of resolution of P–T reading.

The fit to the experimental reversal brackets for the dehydration of *natural* talc requires 600–900 J/mol reduction in the ΔH_f° value from that of synthetic talc. This is, however, too small a difference to be detected by calorimetric measurements. If the nature and density of defects of the synthetic and natural crystals used in this study can be characterized by TEM studies, then the difference in their enthalpies of formation, as required by the phase equilibrium data, can be used to constrain the defect formation energies.

4. Calculations of additional equilibria and phase diagram in the MSH system

4.1. Equilibrium talc + kyanite = pyrope + 3 coesite + H_2O (TKPCV)

The coexistence of talc plus kyanite, with or without pyrope and coesite has been reported from the high pressure metamorphic terrains of the western Alps [4,5,7]. We have calculated this equilibrium using the thermodynamic properties of talc and coesite retrieved in this study and by Bose and Ganguly [21], respectively, along with the optimized thermodynamic data of kyanite and pyrope from the data bases of both Berman [16] and Saxena et al. [32], and of H_2O from Delany and Helgeson [8]. The results are illustrated in Fig. 4, along with the equilibria talc (synthetic) = 3 enstatite + quartz + H_2O, as determined in this work, and quartz = coesite [21]. Also shown for comparison are the experimental results by Chopin [33] on the *TKPCV* equilibrium. The calculated equilibrium using the thermochemical values of pyrope and kyanite from Saxena et al. [32], which is illustrated in Fig. 4 as a solid line, is in very

good agreement with the experimental constraints, whereas that using the pyrope and kyanite values from Berman [16], which is illustrated by a dashed line, violates the experimental data.

4.2. Equilibria involving antigorite and 'phase A'

Besides talc, antigorite ($Mg_{48}Si_{34}O_{85}(OH)_{62}$) is another hydrous sheet silicate of interest in the MSH system, especially in subduction zone environments. In view of the invalidity of the linear compressibility of talc reported in the self-consistent data bases [15,16], as discussed above, it is highly unlikely that the equilibrium relations of antigorite, calculated with the same type of linear compressibility data reported in these data bases, would be reliable. We have, thus, calculated the equilibrium relations of antigorite (Atg) in the MSH system making two alternative assumptions about its compressibility; namely, that: (a) it has a compressibility similar to that of talc, and (b) its compressibility, as deduced by Berman [16], has the same error as that of talc. In the second case, the compressibility of antigorite is represented by a combination of the compressibility given by Berman and a correction factor (Table 3). It is found, however, that the calculated P–T location of the equilibrium Atg = Fo + Ta + H_2O according to assumption (a) is incompatible with the experimental determination of this equilibrium by Evans et al. [34], whereas that according to assumption (b) is in excellent agreement with these experimental results. We have, thus, accepted the results of the calculation of antigorite phase equilibria based on assumption (b) about its compressibility behavior. The calculated equilibria, which radiate from the phase A- and quartz-absent invariant point at low pressure, are as follows:

31 Ta + 45 Fo = Atg + 135 En	(A,Q,V)
Atg = 18 Fo + 4 Ta + 27 H_2O	(A,Q,En)
Atg = 20 En + 14 Fo + 31 H_2O	(A,Q,Ta)
Atg + 14 Ta = 90 En + 45 H_2O	(A,Q,Fo)
Ta + Fo = 5 En + 3 H_2O	(A,Q,Atg)

At high pressures, water is known to be stabilized in what are collectively referred to as 'dense hydrous magnesian silicates' (DHMS). For the lack of complete information on their structural data, various members in this group have been called phase A, B, C, D, etc. Phase A, which has the stoichiometry $Mg_7Si_2O_8(OH)_6$, appears at the lowest pressure among the DHMS phases. Luth [35] determined the equilibrium 5 Fo + 3 H_2O = Phase A + 3 clino-enstatite (Ta,Q,Atg) in a multi-anvil apparatus. The P–T trajectory of this equilibrium intersects the dehydration equilibrium of antigorite (A,Q,Ta) at ~ 70 kbar, almost immediately after inversion of otho- to clino-enstatite. This intersection represents the Ta- and quartz-absent invariant point (Ta,Q) in the MSH system. According to the Schreinemaker's principle, each invariant point in the MSH system must define the intersection of 5 non-degenerate univariant equilibria. Following simple algebraic procedure, one obtains the three other univariant equilibria meeting at (Ta,Q) as follows:

5 Atg = 14 Phase A + 142 OEn + 113 H_2O	(Ta,Q,Fo)
3 Atg + 20 Phase A = 142 Fo + 153 H_2O	(Ta,Q,En)
3 Atg + 113 Fo = 31 Phase A + 153 OEn	(Ta,Q,A)

In order to calculate the above equilibria involving phase A, the thermodynamic functions (H°, S°, Cp°, α and β) of phase A need to be known. Since thermochemical data of phase A are not available, we have retrieved the Gibbs' free energy of formation (from elements) of phase A as function of pressure and temperature over the range 700–1000°C, 70–100 kbar from the experimental reversal brackets of Luth [35]. In this procedure, we used the thermochemical data for forsterite and high-pressure clinoenstatite from Saxena et al. [32] and water properties from Belonoshko et al. [36]. The retrieved Gibbs free energy value of the phase A along the equilibrium (Ta,Q,Atg) between 70 kbar, 730°C and 95 kbar, 910°C can be expressed as:

$$G(J/mol) = -701{,}4414.4 - 463.869(T) - 323{,}8228(10^{-6})(T^2) + 159{,}34641(10^{-6})(P)$$

where T is in degree Kelvin and P is in bars.

The equilibrium relations among talc, antigorite, phase A, forsterite, enstatite, quartz, coesite and H_2O in the MSH system are illustrated in Fig. 5. Of the equilibria involving hydrous phases, only the equilibria Ta = En + 3 SiO_2 + H_2O and Fo + H_2O = A + En have been constrained experimentally.

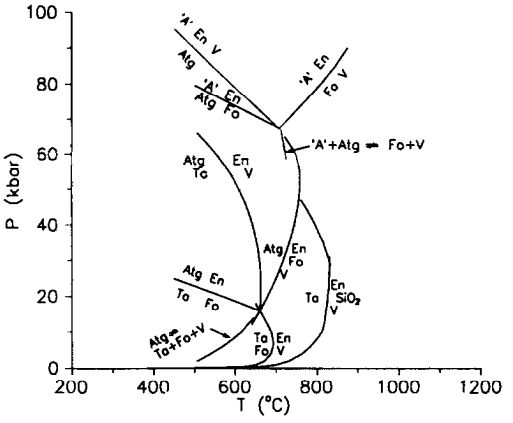

Fig. 5. Experimentally determined and calculated equilibrium relations of talc (Ta), antigorite (Atg), phase A ('A'), enstatite (En), forsterite (Fo) and SiO_2 in the system $MgO–SiO_2–H_2O$ (MSH). The $P–T$ location of the equilibrium Fo + V = 'A' + En is from Luth [35].

Others are calculated, as discussed above. The quartz–coesite equilibrium is taken from Bose and Ganguly [21]. Even though the volumetric properties of antigorite and the thermodynamic properties of phase A are approximate in nature, the calculated phase diagram is still very instructive in the evaluation of the role of antigorite and phase A during subduction of oceanic crust, as discussed below.

5. Applications to subduction processes

We discuss below some applications of the equilibrium relations of talc, antigorite and phase A to the evaluation of the role and fate of structurally bound water subducted by oceanic crust. Along with the phase relations in the MSH system, as deduced above, Fig. 6 shows the stability limits of amphibole in basaltic composition [37], the H_2O-saturated solidus of peridotite [37] and the thermal profiles at the leading edge of old (50 Ma) and young (5 Ma) oceanic plates, each subducting at rates of 3 cm/y and 10 cm/y at an average angle of 26.6° ([38] and Peacock, pers. comm.). In calculating these profiles, which cover a wide range of age and subduction velocities of the oceanic lithosphere, it was assumed that the subducting oceanic crust was characterized by a thermal boundary layer (TBL) with a temperature of 1480°C at a depth of 95 km [39], and that the mantle wedge above the subducting layer was subjected to convection at depths greater than that of the 1000°C isotherm, which is at a depth of ~ 65 km. The sudden increase in temperatures of the thermal profiles at ~ 20 kbar pressure (Fig. 6) is a consequence of the subduction-induced mantle convection.

As shown by Peacock et al. [38], the thermal structure of the hanging walls has relatively minor effects on the $P–T$ path of the leading edge of the subducting slab. They further showed that changing the temperature of the TBL to 1000°C did not significantly affect the temperature at the leading edge of the slab after it had penetrated beyond the depth at which the mantle wedge began to convect. We have chosen to use the temperature profiles calculated numerically by Peacock et al. [38] because these have been shown to agree [40] with the analytical solution at shallow depth within which the mantle wedge does not convect [42] (no analytical solution

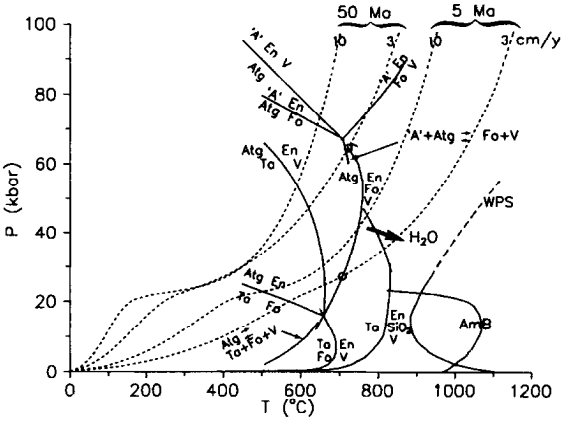

Fig. 6. Comparison of the selected phase relations (MSH) system (Fig. 5) with the thermal profiles (dashed lines) along the leading edge of 50 Ma and 5 Ma old oceanic crust, each subducting at 10 cm/y and 3 cm/y velocities. The $P–T$ location of the equilibrium Fo + V = 'A' + En is from Luth [36]. The thermal profiles are from Peacock et al. [38] and Peacock [pers. commun.]. The sudden change in the slopes of the thermal profiles at ~ 20–25 kbar is due to subduction-induced convection in the mantle wedge. Also shown are the stability limits of basaltic amphibole (AmB) and wet peridotite solidus (WPS), as generated by Davies and Stevenson [37] from the data of Green [42] and Wyllie [47]. The dashed line on WPS represents extrapolation. The range of pressure for the dehydration of antigorite, which is considered to be the major source of water contributing to the partial melting of the mantle wedge, is emphasized by encircled points on the dehydration curve. The vertical ascent path of water released from a dehydrating slab has a $P–T$ slope of ~ 30°C/kbar (~ 10°C/km), which is shown by a heavy arrow.

has been possible for the problem involving a convecting mantle wedge).

The following observations can be made from the phase relations and thermal structure summarized in Fig. 6. (a) Talc that forms at the surface of the oceanic slab will not be carried beyond ~ 25 kbar pressure (~ 75 km depth) because of the presence of excess Mg-rich olivine in the oceanic basalt, which will react with talc to form Atg + En according to the vapor *conserved* reaction 31 Ta + 45 Fo = Atg + 135 En. (b) Antigorite formed by the above process will dehydrate according to Atg = 20 En + 14 Fo + 31 H_2O between ~ 25 and 65 kbar pressure (~ 75–200 km depth), depending on the age and subduction velocity of the slab. In colder slab (≥ 50 Ma), the temperature profile at the leading edge will intersect the vapor *conserved* equilibrium 3 Atg + 113 Fo = 31 phase A + 153 CEn, and the DHMS phase A will then serve as a carrier of water deep into the mantle. (c) Except in a very hot slab, water released from the dehydration of amphibole in basalt will also lead to the formation of antigorite in the overlying mantle wedge, since the intersection of the thermal profile of the leading edge of the slab with the (extrapolated) amphibole dehydration boundary lies at a lower temperature than that of the equilibrium Atg = 20 En + 14 Fo + 31 H_2O. Since the depth of its formation by the above process lies just within the domain of convection of the mantle wedge, antigorite will be dragged downwards, as schematically illustrated in Fig. 7, and would eventually dehydrate between ~ 25 and 65 kbar pressures, depending on the thermal structure of the slab.

Superposition of the P–T condition of wet peridotite solidus (WPS) on the folded thermal structure of the mantle wedge shows that the wet solidus would be folded subparallel to the boundary of the wedge (e.g. [37]), as illustrated schematically in Fig. 7. As a consequence, water released below a certain depth from a subducting slab would reach the wet solidus and induce partial melting of the wedge. This critical depth depends on the details of the thermal structure, which are governed primarily by the age and velocity of subduction. Examination of the stability of antigorite and wet solidus of the mantle wedge in relation to its thermal structure [37] suggests that the depth of release of water from the dehydration of antigorite (~ 75–200 km) would fall

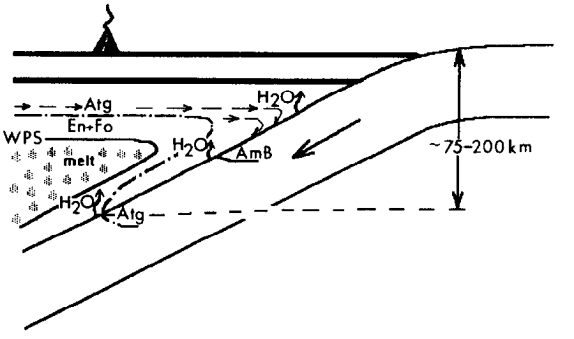

Fig. 7. Schematic illustration of selected dehydration of reactions and magma generation in the subduction zone environment. The mantle wedge convects below the depth (~ 65 km) indicated by arrows. Release of water at shallower depths does not contribute to partial melting of the wedge. At greater depths, water released from the dehydration of basaltic amphibole (AmB) in the subducted slab leads to the formation of antigorite (Atg) in the mantle wedge, which is then dragged downwards by the subduction-induced mantle convection. The reaction boundary En + Fo + H_2O ⇄ Atg is schematically illustrated by heavy dash-dot line. Antigorite is also brought in by the hydrated oceanic crust and can form within the convecting mantle water released by the dehydration of talc in relatively cold slab. The water ascending from the dehydration of antigorite, which takes place between 75 and 200 km, depending on the thermal structure of the leading edge of the slab (Fig. 6), meets the wet solidus of peridotite (WPS) and causes partial melting of the mantle wedge (patterned area), leading to the formation of the volcanoes.

below this threshold depth for the partial melting of the wedge (Fig. 7). Water released from the dehydration of minerals such as chlorite, epidote, brucite, prehnite, etc. [8,43], whose stability limits are exceeded in the leading edge of a subducting slab at shallower depths than that at which the mantle wedge begins to convect would (mostly) escape upwards without either intersecting the P–T condition of the wet solidus or leading to the formation of antigorite within the convecting mantle. Thus, these minerals would have no significant contribution towards magma generation.

If continental sediments that pile up at the continental margin are dragged down to considerable depths by the subducting oceanic lithosphere, as suggested by the $^{10}Be/^{9}Be$ ratio of mineral separates of volcanic arcs [44], then talc in these sediments may be stabilized until the reaction Ta = En + Qz + H_2O is encountered. Subsequent dehydration of talc would lead directly to the process of partial melting of the silicic subducted sediments,

since the wet solidus of these sediments, that is, the wet granite solidus (not shown in Fig. 6), lies at much lower temperatures than that at which the talc dehydration reaction is encountered by the leading edge of the hot slab. In a cold slab (≥ 50 Ma), however, water may be released by the dehydration of talc in the subducted sediments at a lower temperature than the wet solidus of sediments and, consequently, lead to the formation of antigorite in the convecting mantle wedge, which will eventually dehydrate and contribute to the partial melting of the wedge, as discussed above.

Gill [45] made the interesting observation that the height of the volcanic fronts above the Benioff zone falls mostly in the range of 90–158 km and does not exceed the range of ~ 75–200 km. It is now believed that it is the partial melting of the mantle wedge, rather than that of the subducting slab, that is primarily responsible for the magma generation leading to the formation of the volcanic fronts [37,38]. It is interesting to note that the limiting depths for the release of water through the dehydration of antigorite, which should cause partial melting of the mantle wedge (Figs. 6 and 7), closely matches the range of the observed heights of the volcanic fronts above the Benioff zone. It may be recalled that, in our model, antigorite is not only brought along by the subducting slab but that it also forms in the mantle wedge by the reaction of water released by other hydrous phases, most notably amphibole (which is the most abundant hydrous phase), with the peridotite mantle rock. Dilution of water in the vapor phase and solid solution effects would modify the depths of intersection of the thermal profiles of the leading edge of subducting slabs with the dehydration reactions somewhat, but the above scenario seems to provide a satisfactory explanation of the observed height of the volcanic fronts above the Benioff zone.

Acknowledgements

Thanks are due to Dr. Simon Peacock for helpful discussions and providing us with a numerical output of the thermal profiles that were represented graphically in Peacock et al. [41], to Dr. Christian Chopin for providing us with the unpublished data from his doctoral thesis on the dehydration equilibrium of talc plus kyanite, and to Dr. Eric Essene for providing us with the sample of natural talc used in the experimental work. Constructive formal reviews by Drs. Christian Chopin, Robert Luth and Zachary Sharp are gratefully acknowledged. This research was partly supported by a grant from the University of Arizona/NASA Center for the Utilization of Local Planetary Resources. *[RV]*

References

[1] N.L. Bowen and O.F. Tuttle, The system MgO–SiO_2–H_2O, Geol. Soc. Am. Bull. 60, 439–460, 1949.

[2] K. Abraham and W. Schreyer, A talc-phengite assemblage in piemontite schist from Brezovica, Serbia, Yugoslavia, J. Petrol. 17, 421–439, 1976.

[3] W. Schreyer, Metamorphism of crustal rocks at mantle depths: High pressure minerals and mineral assemblages in metapelites, Fortschr. Mineral. 63, 227–261, 1985.

[4] C. Chopin, Talc–phengite: A widespread assemblage in high-grade pelitic blueschists of the Western Alps, J. Petrol. 22(4), 628–650, 1981.

[5] B. Goffé and C. Chopin, High-pressure metamorphism in the western Alps: Zoneography of metapelites, chronology and consequences, Schw. Mineral. Petrogr. Mitt. 66, 41–52, 1986.

[6] W. Schreyer, Subduction of continental crust to mantle depths: Petrological evidence, Episodes 11(2), 97–104, 1988.

[7] C. Chopin, Coesite and pure pyrope in high-grade blueschists of the Western Alps: A first record and some consequences, Contrib. Mineral. Petrol. 86(2), 107–118, 1984.

[8] J.M. Delany and H.C. Helgeson, Calculation of the thermodynamic consequences of dehydration in subducting oceanic crust to 100 kb and >800°C, Am. J. Sci. 278, 638–686, 1978.

[9] B.W. Evans and S. Guggenheim, Talc, pyrophyllite and related minerals, in: Reviews in Mineralogy, 19, S.W. Bailley, ed., pp. 225–294, Mineralogical Society of America, Washington, D.C., 1988.

[10] C. Chopin, Very high-pressure metamorphism in the Western Alps: Implications for subduction of continental crust, Philos. Trans. R. Soc. London Ser. A 321, 183–197, 1987.

[11] Y. Tatsumi, Migration of fluid phases and genesis of basalt magmas in subduction zones, J. Geophys. Res. 94, 4697–4707, 1989.

[12] D. Lane and J. Ganguly, Al_2O_3 solubility in orthopyroxene in the system MgO–Al_2O_3–SiO_2: A re-evaluation and mantle geotherm, J. Geophys. Res. 85, 6963–6972.

[13] R.F. Geise, P.M. Costanzo and C.J. van Oss, The surface free energies of talc and pyrophyllite, Phys. Chem. Miner. 17, 611–616, 1991.

[14] J.V. Chernosky Jr., H.W. Day and L.J. Caruso, Equilibria in the system MgO–SiO_2–H_2O: Experimental determination of

the stability of Mg-anthophyllite, Am. Mineral. 70, 223–236, 1985.

[15] T.J.B. Holland and R. Powell, An enlarged and updated internally consistent thermodynamic dataset with uncertainties and correlations: The system K_2O–Na_2O–CaO–MgO–FeO–Fe_2O_3–Al_2O_3–TiO_2–SiO_2–C–H_2–O_2, J. Metamorph. Geol. 8, 89–124, 1990.

[16] R.G. Berman, Internally-consistent thermodynamic data for minerals in the system Na_2O–K_2O–CaO–MgO–FeO–Al_2O_3–SiO_2–TiO_2–H_2O–CO_2, J. Petrol. 29, 445–522, 1988.

[17] S. Kitahara, S. Takenouchi and G.C. Kennedy, Phase relations in the system MgO–SiO_2–H_2O at high temperatures and pressures, Am. J. Sci. 264, 223–233.

[18] A.B. Thompson and D.J. Ellis, CaO + MgO + Al_2O_3 + SiO_2 + H_2O to 35 kb: amphibole, talc, and zoisite dehydration and melting reactions in the silica-excess part of the system and their possible significance in the subduction zones, amphibole melting, and magma fractionation, Am. J. Sci. 294, 1190–1229.

[19] A. Belonoshko and S.K. Saxena, A molecular dynamics study of the pressure–volume–temperature properties of super-critical fluids: I. H_2O, Geochim. Cosmochim. Acta 55, 381–387, 1991.

[20] J. Brodholt and B. Wood, Molecular dynamics of water at high temperatures and pressures, Geochim. Cosmochim. Acta 54, 2611–2616, 1990.

[21] K. Bose and J. Ganguly, Quartz–coesite transition revisited: Revised experimental determination at 500–1200°C and retrieved thermochemical properties, Am. Mineral. 80, 231–238, 1995.

[22] H.W. Day and H. Halbach, The stability field of anthophyllite: The effect of experimental uncertainty on permissible phase diagram topologies, Am. Mineral. 64, 809–823, 1979.

[23] H.W. Day, J.V. Chernosky Jr. and H.J. Kumin, Equilibria in the system MgO–SiO_2–H_2O: a thermodynamic analysis, Am. Mineral. 70, 237–248, 1985.

[24] Z.D. Sharp, E.J. Essene and J.C. Hunziker, Stable isotope geochemistry and phase equilibria of coesite-bearing whiteschists, Doa Maria Massif, western Alps, Contrib. Mineral. Petrol. 114, 1–12, 1993.

[25] H.-J. Massone, Thermodynamische eigenschaften von phasen des systems MgO–Al_2O_3–SiO_2–H_2O (MASH) unter besonderer berücksichtigung von mischkristallreihen, Ber. Dtsch. Mineral. Gesell. 4, 186.

[26] K. Bose, A. Navrotsky and P. Burnley, Calorimetric determination of enthalpies of formation of dense hydrous magnesium silicates in: EOS Trans. Am. Geophys. Union 75, 597, 1994.

[27] B.S. Hemingway, Thermodynamic properties of anthophyllite and talc, Am. Mineral. 76, 1589–1596, 1991.

[28] SPSS-X User's Guide, 3rd ed., 1072 pp., SPSS Inc., Chicago, 1988.

[29] S.N. Vaidya and G. Kennedy, The compressibility of 18 metals to 45 kilobars, J. Phys. Chem. Solids 31, 2329–2345, 1970.

[30] S.N. Vaidya, S. Bailey, T. Pasternack and G. Kennedy, Compressibility of fifteen minerals to 45 kilobars, J. Geophys. Res. 78(29), 6893–6898, 1973.

[31] A.R. Pawley, S.A.T. Redfern and B.J. Wood, Thermal expansivities and compressibilities of hydrous phases in the system MgO–SiO_2–H_2O: talc, phase A and 10-Å phase, Contrib. Mineral. Petrol., in press, 1995.

[32] S.K. Saxena, N. Chatterjee, Y. Fei and G. Shen, Thermodynamic Data on Oxides and Silicates, 428 pp., Springer, Berlin, 1993.

[33] C. Chopin, Les relations de phases dans les metapelites de haute pression, Mémoirs des Sciences de la Terre, Académie de Paris Université Pierre et Marie Curie, No. 85-11, 1985.

[34] B.W. Evans, W. Johannes, H. Oterdoom and V. Trommsdorff, Stability of chrysotile and antigorite in the serpentine multisystem, Schweiz. Mineral. Petrogr. Mitt. 50, 481–492, 1988.

[35] R. Luth, Is phase A relevant to the Earth's mantle?, Geochim. Cosmochim. Acta 59, 679–682, 1995.

[36] A. Belonoshko, P.F. Shi and S.K. Saxena, SUPERFLUID: a FORTRAN-77 program for calculation of Gibbs free energy and the volume of C–H–O–N–S–Ar Mixtures, Computers.

[37] J.H. Davis and D.J. Stevenson, Physical model of source region of subduction zone volatiles, J. Geophys. Res. 97(B2), 2037–2070, 1992.

[38] S.M. Peacock, T. Rushmer and A.B. Thompson, Partial melting of subducting oceanic crust, Earth Planet. Sci. Lett. 121, 227–244, 1994.

[39] C.A. Stein and S. Stein, A model for the global variation in oceanic depth and heat flow with lithosphere age, Nature 359, 122–129, 1992.

[40] S. Peacock, Thermal and petrological structure of the subduction zone, in: G.E. Bebout, ed., AGU Geophysical Monograph (in review), 1996.

[41] P. Molnar and P. England, Temperatures, heat flux and frictional stress near major thrust faults, J. Geophys. Res. 95, 4833–4856.

[42] D.H. Green, Experimental melting studies on a model upper mantle composition at high pressures under water-saturated conditions, Earth Planet. Sci. Lett. 19, 37–53, 1973.

[43] R.N.Anderson, S. Uyeda and A. Miyashiro, Geophysical and geochemical constraints at the converging plate boundaries — part I: Dehydration in the downgoing slab, Geophys. J. R. Astron. Soc. 44, 333–357, 1976.

[44] J. Morris and F. Tera, ^{10}Be and ^{9}Be in mineral separates and whole rocks from volcanic arcs: Implications for sediment subduction, Geochim. Cosmochim. Acta 53, 3197–3206, 1989.

[45] J. Gill, Orogenic Andesites and Plate Tectonics, 390 pp., Springer, New York, 1981.

[46] S.R. Bohlen and A.L. Boettcher, The quartz ⇄ coesite transformation: A precise determination and the effects of other components, J. Geophys. Res. 87(88), 7073–7078.

[47] P.J. Wyllie, Magmas and volatile components, Am. Mineral. 64, 469–500, 1979.